Geophys. J. Int. (2006) **166,** 1259–1269 doi: 10.1111/j.1365-246X.2006.03053.x

Crustal structure and local seismicity in western Anatolia

Nihal Akyol,[1] Lupei Zhu,[2] Brian J. Mitchell,[2] Hasan Sözbilir[3] and Kıvanç Kekovalı[4]

[1]*Department of Geophysics, Engineering Faculty, Dokuz Eylül University Dokuz Eylül Üniversitesi, Mühendislik Fakültesi, Jeofizik Müh. Bölümü, Tınaztepe kampüsü,* 35160 *Buca/Izmir, Turkey. E-mail: nihal.akyol@deu.edu.tr*
[2]*Department of Earth & Atmospheric Sciences, Saint Louis University, MO, USA*
[3]*Department of Geology, Engineering Faculty, Dokuz Eylül University, Turkey*
[4]*Kandilli Observatory and Earthquake Research Institute, Boğaziçi University, Turkey*

Accepted 2006 April 26. Received 2006 March 25; in original form 2005 February 3

SUMMARY

Western Anatolia is one of the most seismically active continental regions in the world and much of it has been undergoing NS-directed extensional deformation since Early Miocene time. In a cooperative study, seismologists from Saint Louis University, USA and Dokuz Eylül University, Turkey, deployed five broad-band and 45 short-period seismic stations in western Anatolia between 2002 November and 2003 October. The present paper uses data collected by this network and the data from five permanent stations operated by the Kandilli Observatory and Earthquake Research Institute to map the hypocentral distribution of local earthquakes and to determine crustal structure of western Anatolia. We obtained a 1-D *P*-wave crustal velocity model using a generalized scheme for simultaneously obtaining earthquake locations and a crustal velocity model. Our velocity model is characterized by crustal velocities that are significantly lower than average continental values. The low velocities may be associated with high crustal temperatures, a high degree of fracture, or the presence of fluids at high pore pressure in the crust. We located 725 local earthquakes and classified them in three categories. We found that the level of seismic activity in western Anatolia is higher than previously reported. Station delays resulting from the inversion process correlate with near-surface geology and the thickness of sediments throughout the region. The hypocentral distribution of the events indicates that peak seismicity for the region occurs at depths of about 10 km.

Key words: crustal structure, seismicity, tomography, velocity model, western Anatolia.

1 INTRODUCTION

Our region of study in western Anatolia (Figs 1 and 2), is a part of the 'Aegean Extensional Province' and is one of the most seismically active continental regions of the world. The current extension oriented approximately N–S is occurring at a rate of 30–40 mm yr^{-1} (McKenzie 1978; Taymaz *et al.* 1991) in the region, and has replaced the Palaeocene orogenic contraction (e.g. Şengör *et al.* 1985, Taymaz *et al.* 1991; Seyitoğlu & Scott 1996; Bozkurt 2001). During the Early–Middle Miocene period thick volcano-sedimentary associations were formed within approximately NS-trending fault-bounded continental basins under an E–W extensional regime (Yılmaz *et al.* 2000). After starting N–S extension, intracontinental plate alkaline volcanic province of western Anatolia was formed during Late Miocene to Quaternary time (e.g. Aldanmaz 2002; Tonarini *et al.* 2005).

Approximately E–W trending grabens and their basin-bounding active normal faults are the most prominent neotectonic features of Western Anatolia (Bozkurt 2001). Geological observations implied that the thickness of the Neogene sediments in the Gediz Graben (GG, in Fig. 2) is about 1.3–1.5 km, measured to the detachment fault, which forms the contact between the Neogene sediments and metamorphic rocks (Bozkurt & Sözbilir 2004). Analysis of gravity data had revealed that the maximum thickness of sedimentary cover is between 2.5 and 3.5 km in the Buyuk Menderes Graben (BMG, in Fig. 2), and between 0.5 and 2.0 km in the Gediz Graben (GG, in Fig. 2) (Sari & Salk 2006).

Although there has been extensive study of the near-surface geology of this unique region, research on deep crustal structure and earthquake activity has been hampered by sparse coverage of seismic stations. The Department of Earth and Atmospheric Sciences at Saint Louis University and the Department of Geophysical Engineering at Dokuz Eylul University, in late 2002, began a cooperative seismological study of western Anatolia in an effort to better understand the crustal structure and the details of earthquake activity in the region. This paper presents results of our study of the extensive earthquake activity in western Anatolia that is covered by, and adjacent to the recently deployed regional network.

In this study, VELEST (Kissling *et al.* 1994) inversion algorithm was used to solve the hypocentre-velocity model and associated station delay problems for the region. Originally written in 1976 by W.L. Ellsworth and S. Roecker for seismic tomography studies, it

© 2006 The Authors
Journal compilation © 2006 RAS

Downloaded from https://academic.oup.com/gji/article/166/3/1259/748243 by Dokuz Eylul University Library (DEU) user on 02 September 2021

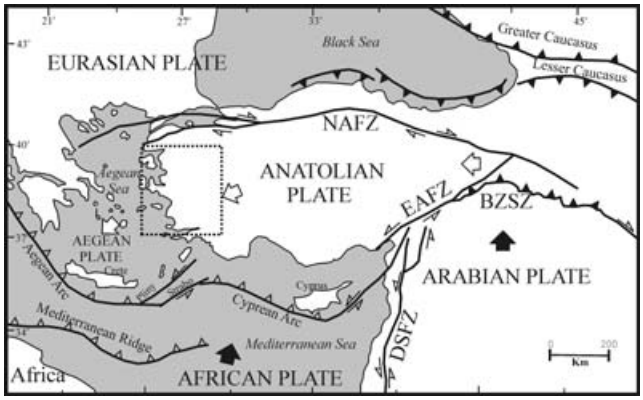


Figure 1. Simplified tectonic map of Turkey showing major neotectonic structures (modified from Barka & Reilinger 1997; Kiratzi & Louvari 2001; Bozkurt & Sözbilir 2004), DSFZ: Dead Sea Fault Zone, EAFZ: East Anatolian Fault Zone, NAFZ: North Anatolian Fault Zone. Heavy lines with half arrows are strike-slip faults with the arrows showing relative movement sense. Heavy lines with filled triangles show major folds and thrust belts with the triangles indicating the direction of convergence. Heavy lines with open triangles indicate an active subduction zone. Bold filled arrows indicate the movement directions of the African and Arabian plates relative to Eurasia. Open arrows indicate the relative motions of the Anatolian and Aegean plates. The area with dashed line shows the region of Fig. 2.

has been modified or used by several authors (i.e. Kissling & Lahr 1991; Castillo & Ellsworth 1993; Ciaccio & Chiarabba 2002; Husen *et al.* 2003).

2 DATA COLLECTION AND PROCESSING

Western Anatolia Seismic Recording Experiment (WASRE) network of 45 short-period and five broad-band stations lasted from November 2002 to October 2003. The IRIS/PASSCAL instrument centre provided 24 L22 sensors and Reftek 72A recorders with a peak sensitivity at 2 Hz and Saint Louis University (SLU) provided five sets of broad-band STS-2 sensors and Reftek-72A recorders. All stations recorded 24-bit data continuously at 40 samples per second. This digitization rate provides sampling resolution that permits accurate event locations.

We deployed 20 high-frequency instruments as a linear array with an inter-station distance that varied between 2 and 3 km depending on the terrain and noise characteristics of station sites. During the first five months of recording we deployed the instruments along the northern half of the linear profile shown in Fig. 2. We deployed one broad-band instrument (station BOZ) on crystalline rock site on Bozdag at the central point of the first linear array where noise level is very low. During the N–S extension period major

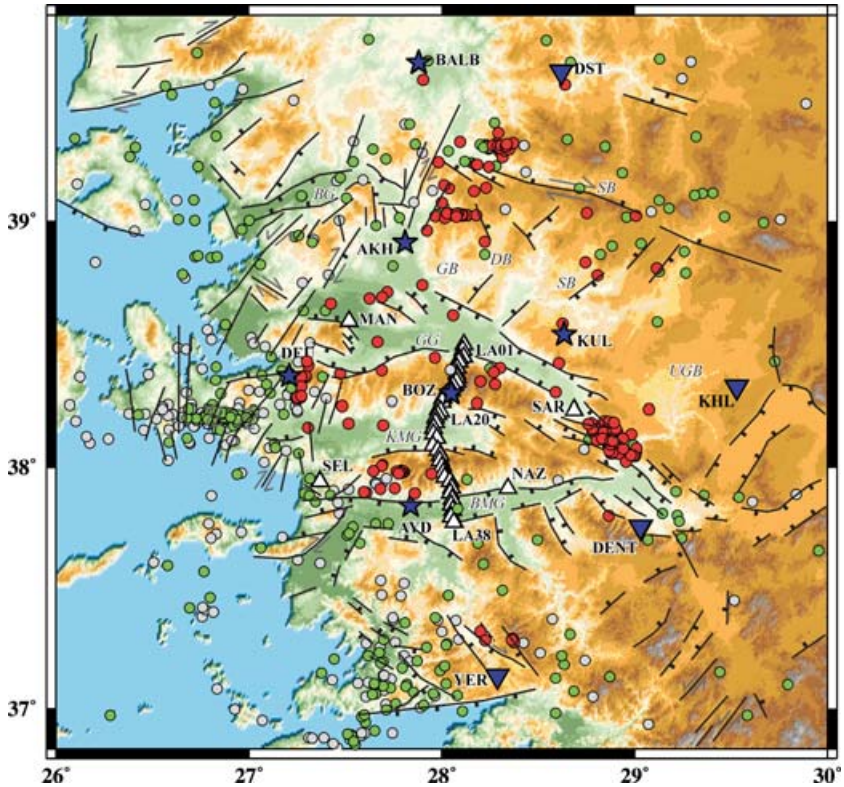


Figure 2. Map showing earthquake locations in western Anatolia between 2002 November and 2003 October. All hypocentre locations were classified into three different categories (Table 3). A, B and C-class events are shown by red, green and grey dots, respectively. Tectonic features were modified from Şengör *et al.* (1985), Şengör (1987), Konak & Şenel (2002), Şaroğlu *et al.* (1992) and Bozkurt (2000). GG: Gediz Graben, KMG: Kucuk Menderes Graben, BMG: Buyuk Menderes Graben, BG: Bakircay Graben, SB: Simav Basin, GB: Gordes Basin, DB: Demirci Basin, and UGB: Usak-Gurle Basin. Grey parallel lines with arrows represent strike slip movements. White triangles and stars represent short-period and broad-band instruments of the WASRE network, respectively. BALB is broadband and DST, KHL, DENT, YER are short-period stations operated by KOERI.

Downloaded from https://academic.oup.com/gji/article/166/3/1259/748313 by Dokuz Eylul University Library (DEU) user on 02 September 2021

breakaway faults began to form around Bozdag, located in the central part of the region (Yılmaz *et al.* 2000). After 5 months we moved the high-frequency instruments of the first linear array so to cover the southern half of the profile in Fig. 2, yielding a total coverage for the linear array of about 100 km. The instruments lay in that configuration for the remaining months of recording. The linear array traversed two prominent E–W trending grabens in western Turkey: the Buyuk Menderes and the Kucuk Menderes Graben (KMG). Four high-frequency and five broad-band instruments were deployed as a regional array. Data from the regional array instruments, plus selected data from the linear array stations were used to locate local events. Because of the proximity of the stations in the linear array to one another we evaluate only high-quality records from those stations to obtain better earthquake locations. In addition, noise levels for array stations in the grabens were significantly higher (by a factor of 3) than for those on the horsts, leading to poor signal-to-noise levels for many of those stations.

First *P*-wave arrival times were obtained by careful visual inspection. To increase the number of *P* arrivals, data from five KOERI stations were also used in the location processes. During the experiment, approximately five events were detected per day. By restricting locations to those events recorded by at least seven stations, we located 902 events using 11 680 *P*-wave arrivals. Of those events, 725 were local earthquakes. Accurate timing of recordings were ensured by frequently synchronizing recorder's internal clock with the GPS time. Time drifts were recorded and were used to make time corrections to waveform data. In most cases, the corrections are less than 10 ms.

The first locations of the local events were obtained using the computer program ELOCATE (Hermann 2004). For this step, we used the velocity model of Kalafat *et al.* (1987) routinely used by the KOERI (Table 1). Following the first location process, well-located events with *rms* values smaller than 0.9 s, azimuthal gap smaller than 180°, and record number greater than 8 were used to determine 1-D minimum *P*-wave velocity model for the region of study. We used the events which have at least two records in each of the hypocentral distance ranges of 0–100 km and 100–200 km to increase the depth resolution of the locations. We then used VELEST (Kissling *et al.* 1994) inversion algorithm, to solve for hypocentral locations, the minimum 1-D velocity model, and associated station delays using only *P*-wave arrivals for all selected events. Finally, a smaller subset of 245 events was located by selecting the events with average residuals smaller than 1.0 s and the records with station residuals smaller than 1.0 s, during the inversion processes. Since the generalized inverse scheme does not automatically adjust layer thickness (Kissling *et al.* 1995), the appropriate layering of the model was found by trial-and-error process.

Table 1. The velocity model used by KOERI for western Anatolia (Kalafat *et al.* 1987).

Depth (km)	*Vp* (km s^{-1})
0.0	4.50
5.4	5.91
31.6	7.80
89.2	8.30

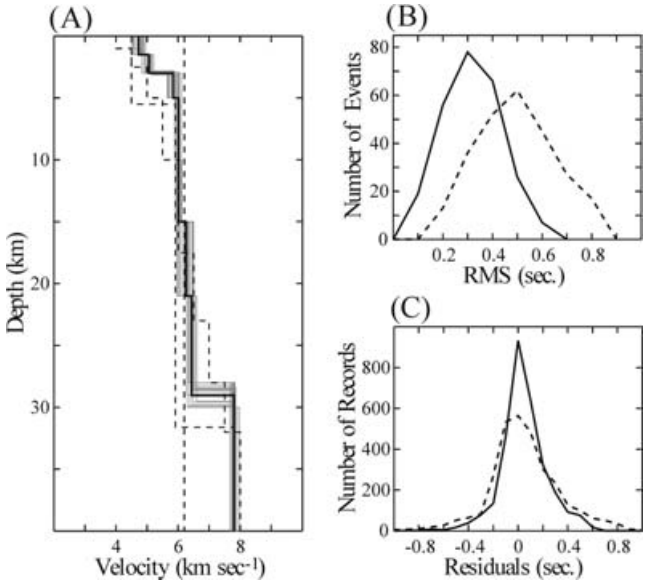


Figure 3. (a) The minimum 1-D *P*-wave velocity model (dark-thick solid line),three initial models (grey-dashed lines) and last convergent 25 velocity models (grey solid lines), (b) *rms* values, and (c) station residuals of 245 events used in the inversion. Solid and dashed lines represent final and preliminary location results, respectively.

3 RESULTS

3.1 Crustal velocity model

Three different velocity models were used as initial models for the inversion: The first is a model obtained by finer sampling of the model which is routinely used by KOERI (Table 1), the second is generated by using available geological information on the crustal structure and the last is a velocity model with constant velocity. These three initial models and the resulting minimum 1-D velocity model together with last convergent 25 models are given in Fig. 3(a). The term 'minimum' thereby denotes that the minimum 1-D model leads to a minimum average of *rms* values for all earthquakes (Husen *et al.* 2003). The minimum 1-D velocity model is obtained by trial and error process with various initial velocity models and with different combinations of damping factors, in order to prove the stability of the results. After several iteration tests, final damping parameters for origin time, *x*, *y*, *z* coordinates and station corrections are chosen as 0.01 and for velocity 1.00 (e.g. Kissling *et al.* 1995). Final *rms* value and data variance of the solution are 0.4 s and 0.5 s, respectively. Final averages of adjustments for origin time, latitude, longitude and depth values are 0.018 s, 0.021, −0.037 and 0.042 km, respectively. The averaged *rms* of event residuals and its standard deviation were reduced by 36 and 33 per cent, respectively (Fig. 3b). The averaged station residual is 0.046 s and the standard deviation reduction is 30 per cent (Fig. 3c).

The diagonal elements of the velocity resolution matrix range between 0.94 and 0.98 and standard deviations of the velocity values are confined within ±0.17 km s^{-1}. The large deviations indicate of significant lateral variation in crustal velocity structure. The velocities at shallow depths (<3 km) are not well constrained due to a lack of head waves and refracted waves that sample shallow depths (Fig. 4). Our data set had also showed that local earthquake tomography in western Anatolia cannot resolve the Moho topography since seismicity is mostly restricted to the upper crust (Fig. 4). For that reason the uppermost mantle velocity and Moho depth were constrained, respectively, to be 7.8 km s^{-1} and 29.0 km using the

© 2006 The Authors, *GJI*, **166,** 1259–1269
Journal compilation © 2006 RAS

Downloaded from https://academic.oup.com/gji/article/166/3/1259/748313 by Dokuz Eylul University Library (DEU) user on 02 September 2021

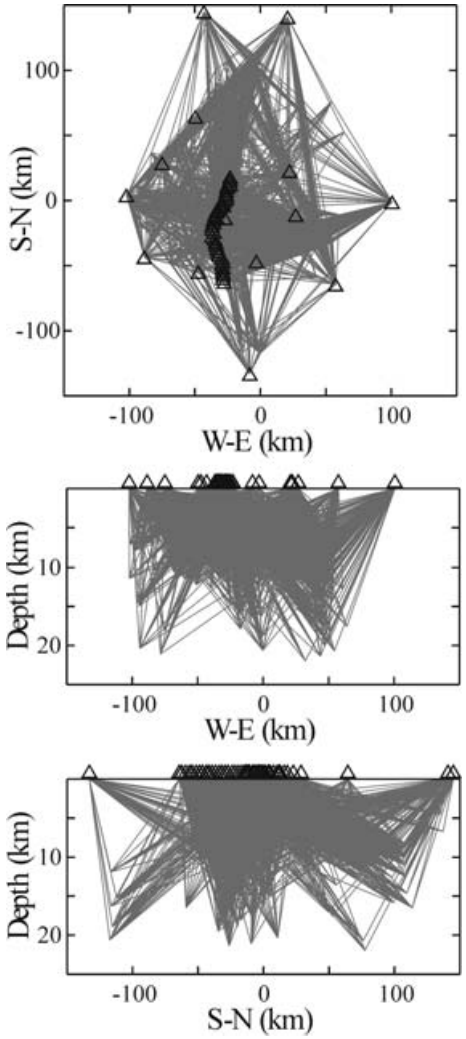


Figure 4. Ray coverage of 245 events located by VELEST (Kissling *et al.* 1994).

velocity model in Table 1 (Kalafat *et al.* 1987) and the model we obtained from receiver function analysis (Zhu *et al.* 2006a), respectively. *Pn* tomographic works results from Hearn & Ni (1994) and Al-Lazki *et al.* (2004) have implied that chosen value of *Pn* velocity (7.8 km s^{-1}) is about the average value, although they pointed out the *Pn* variations for the region.

During the hundreds of iterations of inversion, the VELEST scheme had tried to generate low-velocity zone (LVZ) for the depth values of 10–15 km. We prefer not to use a velocity model with a LVZ since it may introduce some computational instabilities in the ray tracing and, therefore, the location inversion (e.g. Kissling *et al.* 1995). The LVZ appears to only have an effect of 300 m or less in the locations. Additionally, a model with a LVZ is not likely to represent the average velocity structure for the entire region.

The 1-D minimum *P*-wave velocity model in Fig. 3(a) shows four layers between depths of 3 and 29 km, the velocity being 6.25 km s^{-1} at depths between 15 and 21 km. The data we have that pertains to the depth range 21–29 km (the lowermost crust) suggests that it is only about 6.43 km s^{-1}. Christensen & Mooney (1995) suggest 6.44±0.21 km s^{-1} as a global average of crustal velocities.

Table 2. Station delays of the minimum velocity model.

Sta. Code	Lat. (N)	Long. (E)	Elev. (m)	Record no.	Sta. delays
AKH	38.9149	27.8081	128	32	0.27
AYD	37.8407	27.8374	86	73	0.54
BALB[a]	39.6400	27.8800	120	51	−0.03
DENT[a]	37.7540	29.0330	637	183	0.02
DEU	38.3710	27.2078	248	73	0.07
DST[a]	39.6040	28.6190	625	94	0.44
KHL[a]	38.3240	29.5290	940	191	0.30
KUL	38.5401	28.6339	700	96	0,13
LA01	38.4987	28.1135	130	16	0.25
LA02	38.4753	28.1107	194	11	0.12
LA03	38.4497	28.1136	298	07	–
LA04	38.4428	28.0915	654	13	0.11
LA05	38.4288	28.0903	802	16	0.08
LA06	38.4036	28.0804	1043	11	0.08
LA07	38.3805	28.0793	1093	46	0.07
LA08	38.3650	28.0807	1147	03	–
LA09	38.3467	28.0789	1164	05	–
LA10	38.3342	28.0603	1177	63	0.09
LA11	38.3112	28.0521	1210	05	
LA12	38.3022	28.0347	1219	07	
LA13	38.2956	28.0213	989	30	0.11
LA14	38.2801	28.0066	384	26	0.14
LA15	38.2678	28.0012	293	11	0.06
LA16	38.2391	27.9835	186	27	0.20
LA17	38.2270	27.9920	165	02	–
LA18	38.2167	27.9779	156	03	–
LA19	38.2027	27.9680	138	02	–
LA20	38.1841	27.9687	129	82	0.25
LA21	38.1619	27.9573	127	41	0.22
LA22	38.1404	27.9582	169	126	0.16
LA23	38.1196	27.9748	231	38	0.18
LA24	38.0909	27.9567	400	07	–
LA25	38.0710	27.9784	564	15	0.15
LA26	38.0495	27.9891	985	174	0.12
LA27	38.0301	27.9929	753	13	0.14
LA28	38.0055	28.0027	652	04	–
LA29	37.9815	28.0095	699	01	–
LA30	37.9607	28.0168	719	199	0.15
LA31	37.9413	28.0439	579	01	–
LA32	37.9148	28.0514	280	10	0.23
LA33	37.8937	28.0439	226	69	0.27
LA34	37.8692	28.0524	142	99	0.25
LA35	37.8444	28.0509	102	17	0.44
LA36	37.8234	28.0546	77	-	–
LA37	37.7986	28.0522	75	03	–
LA38	37.7731	28.0643	139	174	0.38
LA39	38.4497	28.1136	309	26	0.31
LA40	38.2593	27.9947	244	11	0.15
LA41	38.2128	28.0699	238	22	0.16
MAN	38.5931	27.5184	88	160	0.18
NAZ	37.9134	28.3432	119	24	0.37
SAR	38.2345	28.6859	279	190	0.15
SEL	37.9443	27.3677	49	137	0.65
YER[a]	37.1360	28.2860	729	42	0.14
BOZ	38.3002	28.0495	1216	230	0.00

[a]Stations operated by KOERI.

3.2 Station delays

Table 2 and Fig. 5 show the calculated station delays of the minimum 1-D velocity model. The station delays are the average values for the azimuthally and radially varying time delays at these stations

Downloaded from https://academic.oup.com/gji/article/166/3/1259/748313 by Dokuz Eylul University Library (DEU) user on 02 September 2021

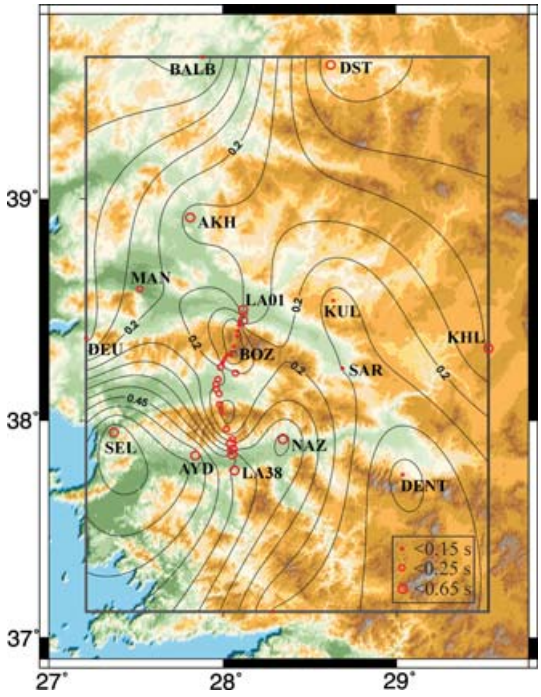


Figure 5. Station delays of the minimum 1-D velocity model (Fig. 2).

relative to the near-surface values of the velocity model. We used only 41 stations and 2962 arrivals for inversion processes and the stations which have less than 10 observations were not used in the inversion processes (e.g. Husen *et al.* 2003). The obtained final station delays varied between −0.03 and +0.65 s. Our reference site is a broad-band instrument on crystalline rock site (station BOZ). Probably since this broad-band site located on good site condition of hard rock in that area, the KOERI broad-band site of BALB has a station delay of −0.03 s, which is less than the reference site. The largest station delay values of 0.65 s for SEL and 0.54 s for AYD sites are directly related to the poor site conditions and sediments thickness underlying these stations, which are located on BMG (Fig. 2). Large delays of KHL and DST stations of KOERI may indicate deeper Moho depth, low average crustal velocities, problem of limited azimuthal coverage of observations and/or systematic phase picking/clock problems at those stations. However, Fig. 5 shows that the station corrections correlate well with the site conditions of the stations, being generally larger for graben stations and smaller for horst stations.

3.3 Earthquake locations

Fig. 6 shows the final and preliminary locations of 245 events. Average differences between final and preliminary locations in latitude, longitude, depth and origin time are 0.705 ± 1.4 km, 1.456 ± 2.0 km, 0.272 ± 6.29 km and 0.101 ± 1.97 s, respectively (Fig. 6c). The systematic shift of values of 1.456 ± 2.0 km is in longitude. This eastward shift is likely due the N–S linear array orientation of the WASRE network. The depth values of final locations indicate that the majority of events occur between 9 and 10 km for the region, while preliminary locations have shallower and also deeper events. Although there is small systematic shift (0.272 km) in depth, the larger standard deviation and larger change in depth is most likely due to lower values in the uppermost and lowermost crust of the KOERI velocity model (Table 1).

The detailed depth distributions of the major cluster lying southeast of the SAR stations are shown in Fig. 7. This figure includes relocated events distribution and fault segmentations nearby the cluster. The located events do not follow mapped faults in the area. Moment tensors of 21 events of the cluster indicate that the cluster occurred on an unmapped left-lateral strike-slip fault (Zhu *et al.* 2006b).

To test for robustness of the new minimum 1-D model and final locations of the events, we systematically shift hypocentre locations to greater depth by 5 km and reintroduce them into the inversion (e.g. Husen *et al.* 1999, 2003). Only a small systematic shift (maximum 650 m) remains after the inversion between the original hypocentre locations and the shifted hypocentre locations. Velocities and station delays are changed by less than 3 per cent denoting the robustness of the minimum 1-D velocity model and locations. The results could not, however, be tested since they lacked arrival-time data from explosions.

Using the new velocity model, we relocated the 725 events for which at least seven recordings were available. All hypocentral locations were classified into three different categories based on location uncertainties (Table 3). The 245 events used in the velocity inversion have the most reliable locations (A-class). B-class events are those without the azimuthal gap restriction. Due to inadequate azimuthal and take-off angle distributions, the depth values were constrained for C-class events. The 725 local earthquakes classified in Table 3 are shown in Fig. 2.

Although we used the new 1-D velocity model for all events, station delays were only applied for the events within the array. The station delays versus increasing hypocentral distances generated linearly increasing shift in the location of the events outside of the array. This indicates that azimuthally and radially varying arrival-time delay at a station is related not only to the near-surface velocities but also to the complexity of the medium traversed by the rays.

To investigate if the seismogenic structures revealed by the WASRE data are similar or different from the much longer term KOERI network observations, we compared location results of these two networks in Fig. 8. During the time period of the experiment, KOERI located 627 events in our area of study, a number which is 98 fewer than the number located in by the WASRE, even though we restricted to those events that have at least seven arrival times. The missing events are most likely caused by the sparse station distribution of the permanent KOERI network. Within the WASRE array configuration, we have three small clusters which are not detected by the KOERI network. On the other hand, both of the networks are able to detect similar broad-scale seismicity patterns in the region. The largest difference between the WASRE and KOERI locations is in event depths. In Fig. 8, we have only given the depths of A- and B-class events in the depth cross-sections (totally 476 events), since the depths of C-class events were constrained. However, the KOERI locations have depth constrain (5 km) for more than 25 per cent of the events (169 events, in Fig. 8b). The peak seismicity depth of A- and B-class events is 8–10 km, while this value is 4–6 km for the KOERI events.

3.4 Event magnitudes

We used simulated Wood–Anderson seismogram amplitudes to determine local magnitudes of the located events. They range between 2.0 and 5.6 (Figs 9a and b). Local earthquakes include 12 events with magnitude equal or greater than 4.0. Table 4 gives the WASRE and KOERI locations of the events that cause seven abrupt increases in seismic activity during the 11 month recording period of the experiment (Figs 9c and d).

Downloaded from https://academic.oup.com/gji/article/166/3/1259/748313 by Dokuz Eylul University Library (DEU) user on 02 September 2021

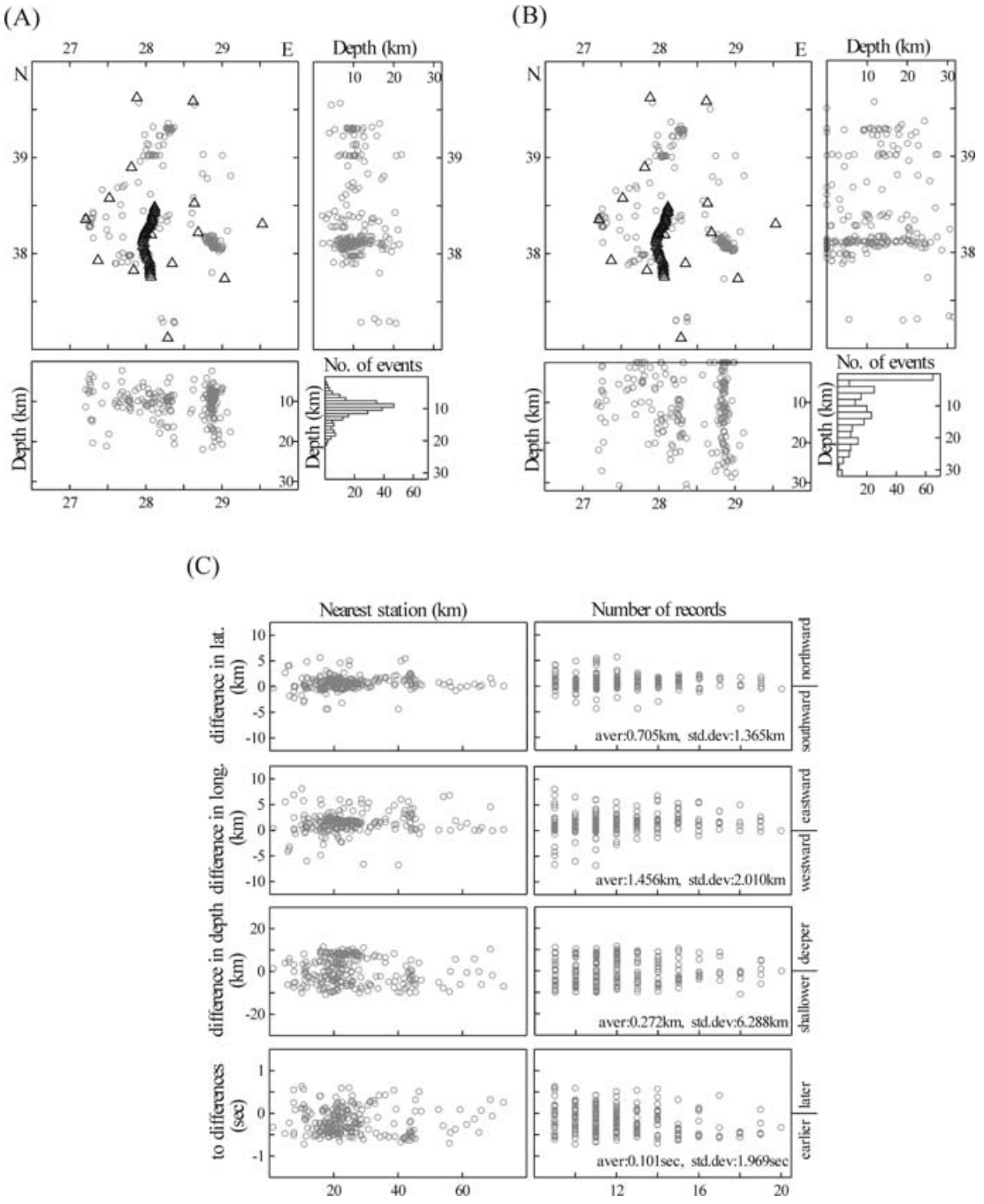


Figure 6. (a) Final event locations, (b) preliminary event locations, and (c) the differences between final and preliminary locations. Positions of the differences relative to preliminary locations are indicated on the right sides of the figures.

Cumulative magnitude distribution versus the time (Fig. 9) shows that the cluster lying south and southwest of station DEU is related to the 2003 October 4 Urla-Izmir earthquake and its aftershocks. An eastern cluster lying southeast of station SAR is related to the 2003 July 23 and 26 Buldan-Denizli earthquakes and the aftershock activities of these earthquakes.

Using A- and B-class events, we calculated earthquake occurrence probabilities and periods for the region (Table 5). The occurrence probability of an event with magnitude equal or greater than 3.0 per day is 100 per cent (Table 5). This means that the WASRE temporary network was able to detect and locate an event whose magnitude value is at least 3.0, per day for the region. We do not have as many events smaller than 2.5 as expected. The paucity of small events is because we required that at least seven stations record each event and thus had difficulty to detect and locate small magnitude events with a sufficient number of stations.

4 DISCUSSION

The velocity model exhibits low values throughout the crust (Fig. 3a and Table 6). The lower crustal velocities in western Anatolia may result from high temperatures, fluids at high pore pressure, or the presence of partial melt. Lower crustal velocities are significantly

Downloaded from https://academic.oup.com/gji/article/166/3/1259/748313 by Dokuz Eylul University Library (DEU) user on 02 September 2021

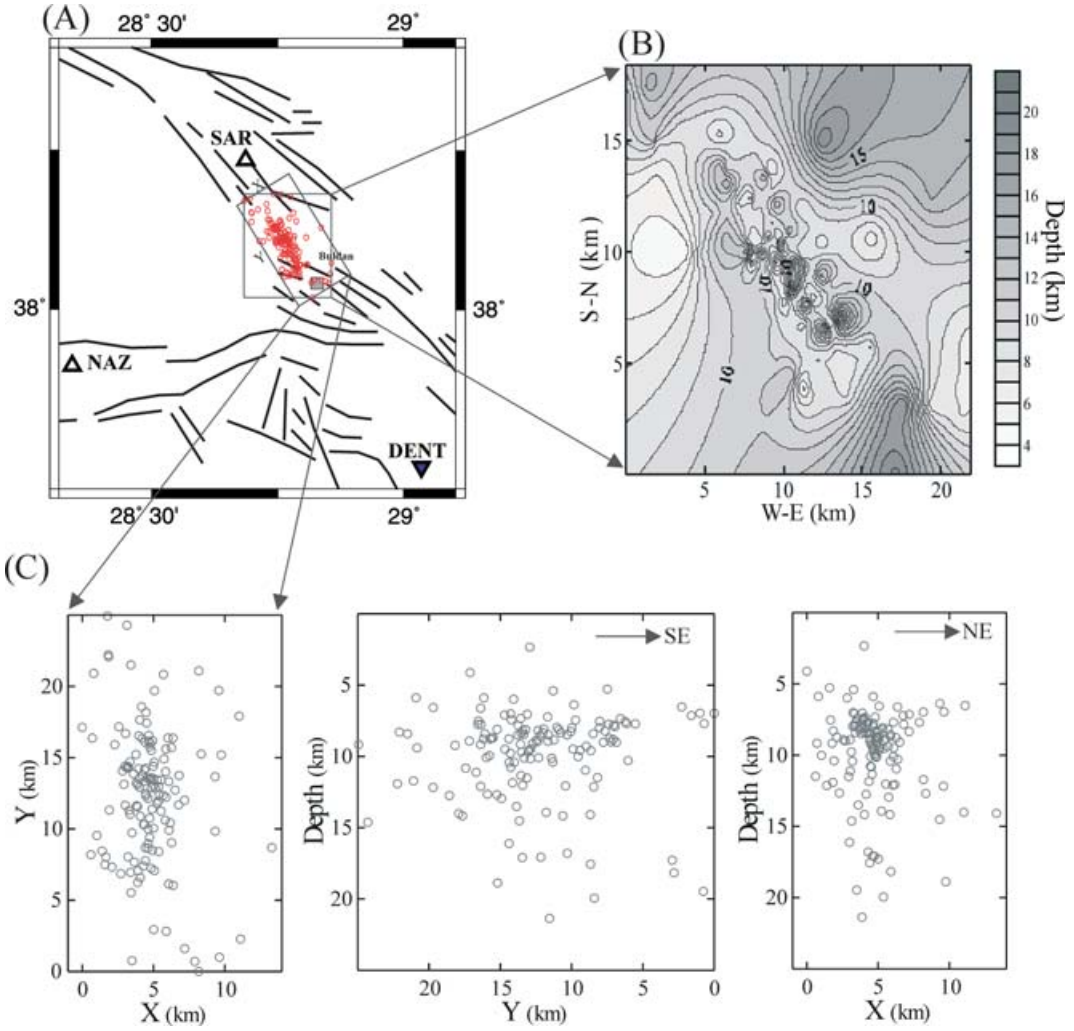


Figure 7. (a) Epicentral distribution of a cluster of events near Buldan and mapped faults in the area (from Şaroğlu *et al.* 1992), (b) depth distribution, and (c) cross-sections of the events in this cluster.

Table 3. Parameter ranges and standard deviations for A-, B- and C-class events.

Parameters range (average ± std. dev.)	A-class events	B-class events	C-class events
rms (s)	0.0–0.7 (0.32 ± 0.17)	0.002–1.0 (0.30 ± 0.26)	0.03–1.5 (0.36 ± 0.31)
Nearest station (km)	0.9–80 (25.71 ± 13.85)	2–145 (49.80 ± 28.16)	4–125 (48.02 ± 24.47)
Depth (km)	2.24–21.96 (10.2 ± 3.6)	1.4–42 (12.95 ± 8.26)	5–20 (8.42 ± 3.64) [a]
Magnitude (ML)	2.0–4.6 (3.0 ± 0.4)	2.1–5.6 (3.2 ± 0.4)	2.4–4.9 (3.2 ± 0.3)
Record number per station	>8 (total 3012)	>7	>7
Event number	245	231	249

[a]Depth fixed for C-class events.

slower, increasing from 6.25 km s^{-1} at 21 km depth to 6.43 km s^{-1} at the Moho. Obtained velocities at the base of the crust are within the bounds of average crustal velocities at high temperature (Christensen & Mooney 1995). The high average heat flow (107 ± 45 mW m^{-2}) with geothermal activity (İlkışık 1995), high rate of seismicity (Bozkurt 2001), intensive faulting (Fig. 2) and extension-related volcanism (Paton 1992) are the main characteristics of the region.

Post-collisional volcanism in western Anatolia displays compositionally distinct magmatic episodes controlled by slab break-off, lithospheric delamination, asthenospheric upwelling with decompressional melting, and oceanic lithospheric subduction as part of the geodynamic evolution of the eastern Mediterranean region throughout the Cenozoic (e.g. Pe-Piper & Piper 2001; Aldanmaz 2002; Dilek 2005). The last episode-forming alkaline volcanic province of western Anatolia is characterized by intracontinental alkali olivine basalts and basanites extruded along localized extensional basins during Late Miocene to Quaternary time (e.g. Aldanmaz 2002; Tonarini *et al.* 2005). The melt source carried no subduction component, and the main magma source was decompressional melting of the asthenospheric mantle flowing in the beneath the attenuated continental lithosphere in the Aegean extensional province.

© 2006 The Authors, *GJI*, **166,** 1259–1269
Journal compilation © 2006 RAS

Downloaded from https://academic.oup.com/gji/article/166/3/1259/748313 by Dokuz Eylul University Library (DEU) user on 02 September 2021

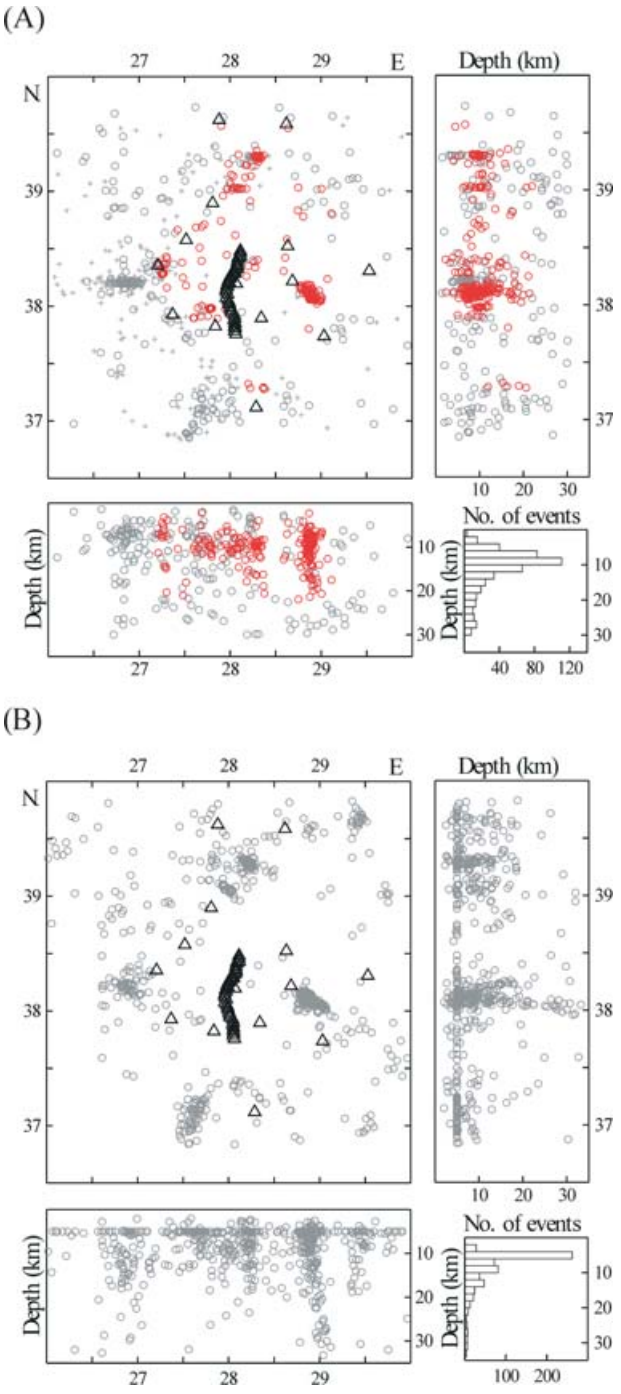


Figure 8. (a) 725 earthquake locations from this study. Red circles, black circles and black cross represent A-, B- and C-class events, respectively. Depth cross-sections only show A- and B-class events (476 events), (b) 627 earthquake locations determined by KOERI.

Lithospheric-scale extensional fault systems provided natural conduits for the transport of uncontaminated alkaline magmas to the surface (Dilek 2005). Trace-element modelling in the region indicated that the mafic magmas formed by variable degrees (∼2–10 per cent) of martial melting and degree of partial melting decreased progressively from early-formed alkali olivine basalts to later basanites. The isotopically depleted nature of the alkaline rocks relative to bulk silicate earth indicates that this enrichment is a recent event related to small degree, multi-stage melting processes that involve local metasomatism of the mantle (Aldanmaz 2002).

Tonarini *et al.* (2005) suggested that the occurrence of intraplate magmas is related to rupture of subducting slab produced by the faster advancement of the Aegean block over Africa with respect to Anatolia in the region. However, lithospheric heating by mantle upwelling and related magma production could support magma-assisted rifting model of initially cold, thick continental lithosphere in western Anatolia (e.g. Kendall *et al.* 2005; Keir *et al.* 2005). The presently exposed detachment faults are truncated and displaced by high-angle normal faults that indicate 'rift mode' extension in western Anatolia during Plio–Quaternary time (e.g. Koçyiğit *et al.* 1999; Bozkurt & Sözbilir 2004).

According to Saunders *et al.* (1998), the extension related magmas may arise from the stretching of the upper mantle. However, these cannot be produced by direct melting of the sublithospheric mantle, since their volume does not constrain the amount of extension. The Kula (station KUL, in Fig. 2) basalts are the most voluminous (∼2.3 km^3), and their high potassium content makes it unlikely that much melt had under plated the lower crust, but the high Mg content rules out significant high level of fractionation (Saunders *et al.* 1998). So, the unusually low velocities may also indicate that fluid-filled faults and fractures in this seismically active region may permeate the crust (e.g. Al-Shukri & Mitchell 1988; Mitchell *et al.* 1997).

Since we lack coverage within the lowermost crust (Fig. 4), we constrained the upper mantle velocity and Moho depth to be 7.8 km s^{-1} and 29.0 km, respectively. The average *Pn* velocity for the entire Aegean region is approximately 7.9 km s^{-1} (Panagiotopoulos & Papazachos 1985), which is lower than the worldwide average continental upper mantle *Pn* velocity of 8.1 km s^{-1} (Mooney & Braile 1989). *Pn* velocity for western Anatolia is suggested to be 7.8 and 7.85 by Kalafat *et al.* (1987) and Horasan *et al.* (2002), respectively. Although, the *Pn* tomographic imaging from Al-Lazki *et al.* (2004) indicated high *Pn* velocity corridors in the eastern and western parts of the Anatolian plate, it reveals an average *Pn* velocity values is about 7.8 km s^{-1} for the region of our interest. They suggested that the very low *Pn* velocity (∼7.5 km s^{-1}) and thinned crust (26–32 km) beneath the Aegean (Makris & Vees 1977) may reflect a very thin to absent mantle lid, where *Pn* propagation is actually sampling asthenospheric rather than lithospheric mantle. According to Hammer *et al.* (2000), slow mantle velocities (7.8–7.9 km s^{-1}) may also be indicative of high upper mantle temperatures.

Şengör *et al.* (1985) suggested that the crust in western Anatolia had thickened to about 50 to 55 km by Early Miocene time as a result of Palaeocene orogenic contraction. The combined crustal thickening and local extension following have led to regional variations in crustal thickness. Mindevalli & Mitchell (1989), using surface waves, give an average crustal thickness of about 34 km for the western part of Anatolia. According to Saunders *et al.* (1998), the crust is about 30 km thick under the KULA region (station KUL, in Fig. 2). Horasan *et al.* (2002) suggest a crustal thickness of 33km in the region. Recent work including receiver function analysis had showed that Moho depth is about 28 and 30 km under the stations BOZ and KUL, respectively (Zhu *et al.* 2006a).

The inversion for our new velocity model (Fig. 3a) and earthquake locations (Fig. 2) also yielded station corrections (Fig. 5) that reflect near-surface geological complexities in the region (Fig. 2). Determinations of larger values of these corrections for stations on grabens filled with thick sediments and relatively lower values for stations on horsts also gives us confidence on the

Downloaded from https://academic.oup.com/gji/article/166/3/1259/748313 by Dokuz Eylul University Library (DEU) user on 02 September 2021

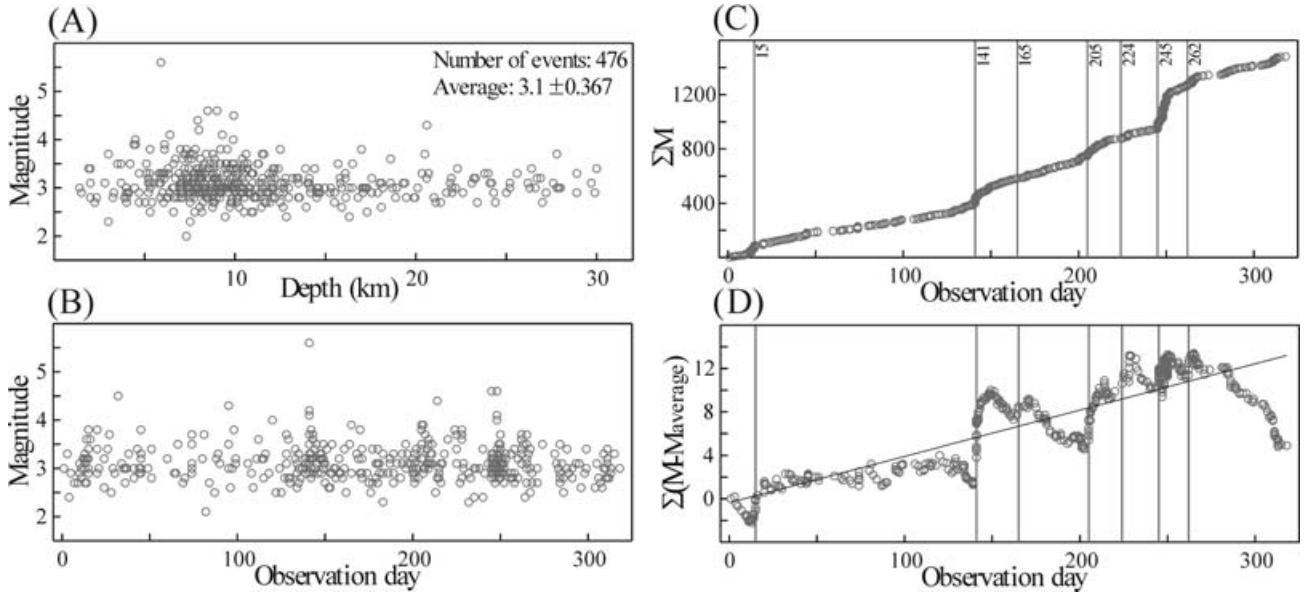


Figure 9. Local magnitude distributions versus (a) event depth and (b) the time. (c) Cumulative magnitudes, and (d) the difference between the cumulative magnitudes and the average magnitude (3.1) versus the time.

Table 4. The WASRE and KOERI locations of the events which cause abrupt increases in the cumulative magnitude values (Figs 9c and d).

Observation day	Date (yr/m/d)	Time (U.T.)	Long. (E)	Lat. (N)	Mag.	Depth (km)	Location
15	021206	12:16:01.38	36.9103	27.6524	3.4	10.4	Gokova
15*		12:16:03	37.121	27.647	3.2	6.19	Bay
141	030410	00:40:16.21	38.1987	26.7478	5.6	5.9	Urla
141*		00:40:16	38.2568	26.8345	5.6	15.8	(Izmir)
165	030504	11:00:35.43	38.2222	26.8657	3.9	4.5	Urla
165*		11:00:33	38.1918	26.8583	4.4	10.0	(Izmir)
205	030613	10:28:57.21	39.3014	28.2267	3.9	4.4	Bigadic
205*		10:28:57	39.3382	28.2633	3.8	7.5	(Balikesir)
224	030702	01:43:36.17	38.0599	29.0045	3.8	6.97	Buldan
224*		01:43:35	38.0602	28.9485	4.0	5.0	(Denizli)
245	030723	04:56:04.45	38.0979	28.8748	4.6	8.49	Buldan
245*		04:56:02	38.1718	28.8533	5.2	5	(Denizli)
262	030809	12:27:59.57	39.3032	28.2854	3.6	8.87	Bigadic
262*		12:27:58	39.3217	28.1735	3.1	7.8	(Balikesir)

*Location parameters obtained by KOERI with duration magnitude scale.

Table 5. Occurrence probabilities and periods based on the first two classes of events.

Magnitude	N	$\sum N$	Pr ($m \geq M$) $\sum N/\Delta t$	Period (day) $\Delta t/\sum N$
$M \geq 5.5$	1	1	0.003145	318
$5.5 > M \geq 5.0$	0	1	0.003145	318
$5.0 > M \geq 4.5$	4	5	0.015723	63.6
$4.5 > M \geq 4.0$	7	12	0.037736	26.5
$4.0 > M \geq 3.5$	55	67	0.210692	4.746269
$3.5 > M \geq 3.0$	251	318	1	1
$3.0 > M \geq 2.5$	150	468	1.471698	0.679487
$2.5 > M \geq 2.0$	8	476	1.496855	0.668067

N: Number of events, Δt: Number of observation days (318).

Table 6. Obtained minimum 1-D velocity model.

Depth (km)	Vp (km s^{-1})	R-diag for the model	Standard deviation
0.0–1.5	4.73	–	–
1.5–3.0	5.06	–	–
3.0–5.0	5.84	0.981	0.124
5.0–15.0	6.00	0.936	0.169
15.0–21.0	6.25	0.962	0.160
21.0–29.0	6.43	0.978	0.123
29.0-[a]	7.80	*	*

[a]Due to a lack of ray coverage below 29 km, we fixed the *Pn* velocity and Moho depth as 7.8 km s^{-1} and 29.0 km, respectively.

velocity model and earthquake locations determined by the inversion process.

725 local earthquakes were located throughout the study area (Fig. 2) in three different categories (Table 3). When we compare the location results of the WASRE and KOERI networks for the same observation time interval, WASRE results show that seismic activity in western Anatolia is 16 per cent higher than previously reported, even if our observation number restriction (at least 7 observations

Downloaded from https://academic.oup.com/gji/article/166/3/1259/748313 by Dokuz Eylul University Library (DEU) user on 02 September 2021

per event). Both of the networks are able to detect major seismogenic structures, although our results indicate a few minor clustered events within the array configuration (Fig. 8). The main difference in the location results is in depth values. The KOERI has much deeper events than our final locations (Fig. 8). This difference is most likely due to the lower velocities for the lowermost crust in the KOERI velocity model (Table 1). The minimum 1-D *P*-wave velocity model in Fig. 3(a) shows four layers between depths of 3 and 29 km, the velocity being 6.25 km s^{-1} at depth range of 15–21 km and 6.43 km s^{-1} at depth range of 21–29 km. However, the model routinely used by KOERI (Table 1) shows the velocity being 5.91 km s^{-1} at depths between 5.4 and 31.6 km s^{-1}.

Şengör (1987) pointed out that all extensional earthquakes in western Anatolia and in the Aegean occur at depths not exceeding about 10 km. This observation may suggest the presence of seismically active low-angle breakaway faults within the upper crust of western Anatolia. The validity of this zone of activity is supported by the many randomly scattered events that we have located on the basin bounding faults (Fig. 2). The depth distribution of well-located A-class events (Fig. 6a) shows that the predominant depth of seismicity is about 9–10 km. On the other hand, Husen *et al.* (2003) suggest that the events with a low number of observations (<8) and no observation within the critical focal depth distance typically show large location uncertainties. Although we have observations greater than 8 for A-class events, only 66 events have at least one *P*-wave arrival at a station within 1.5 focal depth distance and the peak seismicity of those events is slightly deeper (10–11 km).

5 CONCLUSIONS

In summary, the WASRE network consisting of five broad-band and 45 short-period seismic stations, supplemented by five KOERI permanent stations, recorded earthquake activity in western Anatolia from 2002 November to 2003 October. We determined a new crustal velocity model and located earthquakes using *P* waves and the coupled velocity-location program VELEST (Kissling *et al.* 1994).

The results show the crust in the study area is characterized by velocities lower than the global average. The low crustal velocities may be associated with high crustal temperatures, a high degree of fracture, or the presence of fluids at high pore pressure in the crust. The large standard deviation values of the 1-D velocity model indicate significant lateral variation in velocity structure. Station delays which are well correlated with site conditions reveal geological complexities in the region, but also they can only reflect average delays per station for the area within the array configuration.

The short-duration, temporary WASRE network was able to locate an event having magnitude equal and greater than 3.0 per day. Our results show that seismic activity in western Anatolia is higher than previously reported. The hypocentral distribution of the events shows a relation between seismicity and active seismogenic zones in the region. The cumulative earthquake magnitudes with time shows seven abrupt increases in seismic activity, which are related with the clustered events in the region. The peak seismicity depth for the region is about 10 km.

It is obvious that a 1-D velocity model cannot account for all structural complexities in such a region of complicated tectonics. Our analyses also showed that shallow local earthquake tomography in western Anatolia cannot resolve the Moho topography because seismicity is mostly restricted to the upper crust. For that reason, controlled-source seismic data and much more local earthquake data are needed to derive 2-D velocity model and investigate its influence on hypocentre locations. The sparse permanent network stations in the region and short-duration temporary seismic networks are not sufficient for that task.

ACKNOWLEDGMENTS

The authors are grateful to two anonymous reviewers and a *GJI* associate editor who significantly improved the manuscript. We thank Mike Fort, M. Ali Danışman, Oğuz Demir, Zülfikar Erhan, Adem Sömer and Emre Timur for their dedicated efforts in installing and maintaining all of the seismic stations during the course of this study. Our work benefited greatly from the cooperation and support of village officials and many residents of towns and villages throughout western Anatolia. We thank William Ellsworth and Aybige Akıncı for their useful suggestions and Bob Herrmann who provided his codes and advice on computational approaches that facilitated this work. This research was supported by the National Science Foundation (NSF), Office of International Science and Engineering, under Grant OISE 0217493 and by the Scientific and Technical Research Council of Turkey (TUBITAK), the Research Grant Committee of Marine, Terrestrial and Atmospheric Sciences, under Grant YDABAG 102Y015. The epicentre maps were plotted using the GMT code of Paul Wessel and Walter H. F. Smith.

REFERENCES

Aldanmaz, E., 2002. Mantle source characteristics of alkali basalts and basanites in an extensional intracontinental plate setting, western Anatolia, Turkey: implications for multi-stage melting, *Int. Geol. Review,* **44**(5), 440–457.

Al-Lazki, A., Sandvol, E., Seber, D., Barazangi, M., Turkelli, N. & Mohamad, R., 2004. *Pn* tomographic imaging of mantle lid velocity and anisotropy at the junction of the Arabian, Eurasian and African plates, *Geophys. J. Int.,* **158,** 1024–1040.

Al-Shukri, H. & Mitchell, B.-J., 1988. Reduced seismic velocities in the source zone of new Madrid earthquakes, *Bull. seism. Soc. Am.,* **78,** 1491–1509.

Barka, A. & Reilinger, R., 1997. Active tectonics of the eastern Mediterranean region: deduced from GPS, neotectonic, and seismicity data, *Annali Geofisica,* **40,** 587–610.

Bozkurt, E., 2000. Timing of extension on the Büyük Menderes Graben, western Turkey, and its tectonic implications, in *Tectonics and Magmatism in Turkey and the Surrounding Area*, Vol. 173, pp. 385–403, eds Bozkurt, E., Winchester, J.-A. & Piper, J.D.A., Geol. Soc. London Special Publication.

Bozkurt, E., 2001. Neotectonics of Turkey—a synthesis, *Geodinamica Acta,* **14,** 3–30.

Bozkurt, E. & Sözbilir, H., 2004. Tectonic evolution of the Gediz graben: field evidence for an episodic, two-stage extension in western Turkey, *Geological Magazine,* **141,** 63–79.

Castillo, D.-A. & Ellsworth, W.-L., 1993. Seismotectonics of the San Andreas Fault System between Point Arena and Cape Mendocino in Northern California: implications for the development and revolution of a Young transform, *J. geophys. Res.,* **98**(B4), 6543–6560.

Christensen, N.-I. & Mooney, W.-D., 1995. Seismic structure and composition of the continental crust, *J. geophys. Res.,* **100,** 9761–9788.

Ciaccio, M.-G. & Chiarabba, C., 2002. Tomographic models and seismotectonics of the Reggio Emilia Region, Italy, *Tectonophysics,* **344,** 261–276.

Dilek, Y., 2005. Tectonics of post-collisional volcanism in Cenozoic western Anatolia (Turkey), *GSA Annual Meeting Abstracts with Programs,* **37**(7), p. 389.

Hammer, P.-T.-C., Clowes, R.-M. & Ellis, R.-M., 2000. Crustal structure of NW British Columbia and SE Alaska from seismic wide-angle studies: coast plutonic complex to Stikinia, *J. geophys. Res.,* **105,** 7961–7981.

Downloaded from https://academic.oup.com/gji/article/166/3/1259/748313 by Dokuz Eylul University Library (DEU) user on 02 September 2021

Hearn, T.-M. & Ni, J.-F., 1994. *Pn* velocities beneath continental collision zones: the Turkish-Iranian Plateau, *Geophys. J. Int.,* **117,** 273–283.

Hermann, R.-B., 2004. Computer Programs in Seismology, Version 3.30-GSAC, Saint Louis University, USA.

Horasan, G., Gülen, L., Pınar, A., Kalafat, D., Özel, N., Kuleli, S. & Işıkara, A.-M., 2002. Lithospheric structure of the Marmara and Aegean Regions, Western Turkey, *Bull. seism. Soc. Am.,* **92**(1), 322–329.

Husen, S., Kissling, E., Flueh, E.-R. & Asch, G., 1999. Accurate hypocentre determination in the seismogenic zone of the subducting Nazca Plate in Northern Chile using a combined on/offshore network, *Geophys. J. Int.,* **138,** 687–701.

Husen, S., Kissling, E., Deichmann, N., Wiemer, S., Giardini, D. & Baer, M., 2003. Probabilistic earthquake location in complex three-dimensional velocity models: application to Switzerland, *J. geophys. Res.,* **108**(B2), 2077, doi:10.1029/2002JB001778.

İlkışık, O.-M., 1995. Regional heat flow in Western Anatolia using silica temperature estimates from thermal springs, *Tectonophysics,* **244,** 175–184.

Kalafat, D., Gürbüz, C., Üçer, S.-B., 1987. Batı Türkiye'deki Kabuk ve Üst Manto Yapısının Araştırılması, *Turkish Bull. Earthquake Researches,* **59,** pp. 43–64 (in Turkish).

Keir, D., Kendall, J.-M., Ebinger, C.-J. & Stuart, G.-W., 2005. Variations in late Syn-rift melt alignment inferred from shear-wave splitting in crustal earthquakes beneath the Ethiopian Rift, *Geophys. Res. Lett.,* **32,** L23308, doi:10.1029/2005GL024150.

Kendall, J.-M., Stuart, G.-W., Ebinger, C.-J., Bastow, I.-D. & Keir, D., 2005. Magma-assisted rifting in Ethiopia, *Nature,* **433,** 146–148.

Kiratzi, A.-A. & Louvari, E.-K., 2001. On the Active Tectonics of the Aegean Sea and the surrounding lands: in *Proceedings of Symposia on Seismotectonics of the North-Western Anatolia-Aegean and Recent Turkish earthquakes*, pp. 88–95, ed. Taymaz, T., Istanbul Technical University, Turkey.

Kissling, E. & Lahr, J.-C., 1991. Tomographic image of the Pasific Slap under Southern Alaska, *Eclogae Geol. Helv.,* **84,** 297–315.

Kissling, E., Ellsworth, W.-L., Eberhart-Phillips, D. & Kradolfer, U., 1994. Initial reference models in local earthquake tomography, *J. geophys. Res.,* **99**(B10), 19 635–19 646.

Kissling, E., Kradolfer, U. & Maurer, H., 1995. Program Velest User's Guide, Institute of Geophysics, ETH Zuerich.

Koçyiğit, A., Yusufoğlu, H. & Bozkurt, E., 1999. Evidence from the Gediz graben for episodic two-stage extension in western Turkey, *J. geol. Soc. Lond.,* **156,** 605–616.

Konak, N. & Şenel, M., 2002. Geological map of Turkey at 1:500000 scale. General Directorate of Mineral and Research Exploration of Turkey Publication, Turkey.

Makris, J. & Vees, R., 1977. Crustal structure of the Central Aegean Sea and the Islands of Evia and Crete, obtained by Refractional Seismic Experiment, *J. Geophys.,* **42,** 329–341.

McKenzie, D.-P., 1978. Active tectonics of the Alpine-Himalayan Belt: the Aegean Sea and surrounding regions, *Geophy. J. R. astr. Soc.,* **55,** 217–254.

Mindevalli, Y.-Ö. & Mitchell, B.-J., 1989. Crustal structure and possible anisotropy in Turkey form seismic surface wave dispersion, *Geophys. J. Int.,* **98,** 93–106.

Mitchell, B.-J., Pan, Y., Xie, J. & Cong, L., 1997. Lg coda Q variation across Eurasia and its relation to crustal evolution, *J. geophys. Res.,* **102,** 22 767–22 779.

Mooney, W.-D. & Braile, L.-W., 1989. The seismic structure of the continental crust and upper mantle of North America, in *Geology of North America—An Overview*, pp. 39–52, eds Bally, A.-W. & Palmer, A.-R., Geol. Soc. Am., Boulder, Colorado.

Panagiotopoulos, D.-G. & Papazachos, B.-C., 1985. Travel times of *Pn*-waves in the Aegean and surrounding area, *Geophys. J. R. astr. Soc.,* **80,** 165–176.

Paton, S., 1992. Active Normal Faulting, Drainage Patterns and Sedimentation in Southwestern Turkey, *J. geol. Soc. Lond.,* **149,** 1031–1044.

Pe-Piper, G. & Piper, D.-J.-W., 2001. Late Cenozoic, Post-collisional Aegean igneous rocks: Nd, Pb and Sr Izotopic constraints on petrogenetic and tectonic models, *Geol. Mag.,* **138**(6), 653–668.

Sari, C. & Salk, M., 2006. Sediment thicknesses of the western Anatolia graben structures determined by 2D and 3D analysis using gravity data, *J. Asian Earth Sci.,* **26,** 39–48.

Saunders, P., Priestly, K. & Taymaz, T., 1998. Variations in the crustal structures beneath western Turkey, *Geophys. J. Int.,* **134,** 373–389.

Seyitoğlu, G. & Scott, B.-C., 1996. The cause of N–S extensional tectonics in western Turkey: tectonic escape vs back-arc spreading vs orogenic collapse, *J. Geodyn.,* **22**(1), 145–153.

Şaroğlu, F., Emre, Ö. & Kuşçu, I., 1992. Active fault map of Turkey. General Directorate of Mineral and Research Exploration of Turkey Publication, Turkey.

Şengör, A.-M.-C., 1987. Cross-faults and differential stretching of hanging walls in regions of low-angle normal faulting: examples from western Turkey, in *Continental Extensional Tectonics*, pp. 575–589, eds Coward, M.-P., Dewey J.-F. & Hancock, P.-L., Geol. Soc. London Publication.

Şengör, A.-M.-C., Görür, N. & Şaroğlu F., 1985. Strike-slip faulting and related basin formations in zones of tectonic escape: Turkey as a Case Study, in *Strike-slip Faulting and Basin Formation*, pp. 227–264, eds Biddle K.-T. & Christie-Blick N., Soc. Econ. Paleontol. Mineral. Special Publication.

Taymaz, T., Jackson, J. & McKenzie, D., 1991. Active tectonics of the North and Central Aegean Sea, *Geophys. J. Int.,* **106,** 433–490.

Tonarini, S., Agostini, S., Innocenti, F. & Manetti, P., 2005, $d_{11}B$ as tracer of slab dehydration and mantle evolution in western Anatolia Cenozoic magmatizm, *TerraNova,* **17,** 259–264.

Yılmaz, Y., Genç, S.-C., Gürer, O.-F., Bozcu, M., Yılmaz, K., Karacık, Z., Aktunkaynak, Ş. & Elmas, A., 2000. When did the western Anatolian grabens begin to develop? in *Tectonics and Magmatism in Turkey and the Surrounding Area*, pp. 353–384, eds Bozkurt, E., Winchester, J.-A. & Piper, J.-D.-A., Geol. Soc. London Special Publication, 173.

Zhu, L., Mitchell, B.J., Akyol, N., Cemen, I., Kekovali, K., 2006a. Crustal Thickness Variation in the Aegean Region and Its Implications for the Extension of Continental Crust, *J. geophys. Res.,* **111,** B01301, doi:10.1029/2005JB003770.

Zhu, L., Akyol, N., Mitchell, B.-J. & Sozbilir, H., 2006b. Seismotectonics of Western Turkey from high resolution earthquake relocations and moment tensor determination, GRL, **33,** L07316, doi:10.1029/2006GL025842.

Downloaded from https://academic.oup.com/gji/article/166/3/1259/748313 by Dokuz Eylul University Library (DEU) user on 02 September 2021